

PAPER

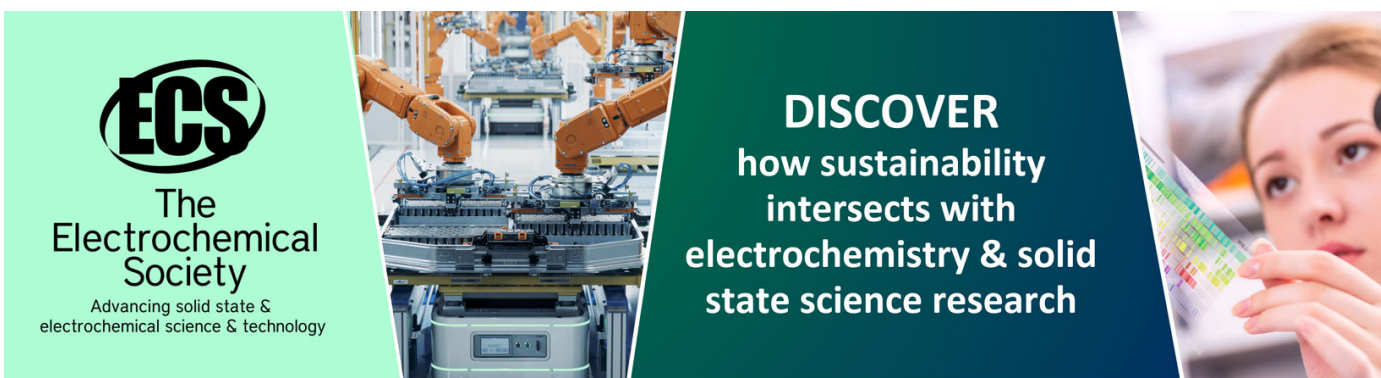
Direct measurement of the effective infrared dielectric response of a highly doped semiconductor metamaterial

To cite this article: Abeer Al Mohtar *et al* 2017 *Nanotechnology* **28** 125701

View the [article online](#) for updates and enhancements.

You may also like

- [THE 5:1 NEPTUNE RESONANCE AS PROBED BY CFEPs: DYNAMICS AND POPULATION](#)
R. E. Pike, J. J. Kavelaars, J. M. Petit *et al.*
- [Spectra of Halo Nuclei](#)
Wang ZhengDa, Wang XiaoBin, Wang XiaoChun *et al.*
- [Two-resonance probe for measuring electron density in low-pressure plasmas](#)
D W Kim, S J You, S J Kim *et al.*



ECS
The
Electrochemical
Society
Advancing solid state &
electrochemical science & technology

DISCOVER
how sustainability
intersects with
electrochemistry & solid
state science research

Direct measurement of the effective infrared dielectric response of a highly doped semiconductor metamaterial

Abeer Al Mohtar¹, Michel Kazan², Thierry Taliercio^{3,4}, Laurent Cerutti^{3,4}, Sylvain Blaize¹ and Aurélien Bruyant¹

¹UTT, ICD-LNIO and STMR—UMR6279 CNRS, 12 rue Marie Curie—CS 42060, F-10004 Troyes, France

²Department of Physics, American University of Beirut, PO Box 11-0236, Riad El-Solh, Beirut 1107-2020, Lebanon

³Univ. Montpellier, IES, UMR 5214, F-34000, Montpellier, France

⁴CNRS, IES, UMR 5214, F-34000, Montpellier, France

E-mail: aurelien.bruyant@utt.fr

Received 9 October 2016, revised 9 January 2017

Accepted for publication 2 February 2017

Published 21 February 2017



Abstract

We have investigated the effective dielectric response of a subwavelength grating made of highly doped semiconductors (HDS) excited in reflection, using numerical simulations and spectroscopic measurement. The studied system can exhibit strong localized surface resonances and has, therefore, a great potential for surface-enhanced infrared absorption (SEIRA) spectroscopy application. It consists of a highly doped InAsSb grating deposited on lattice-matched GaSb. The numerical analysis demonstrated that the resonance frequencies can be inferred from the dielectric function of an equivalent homogeneous slab by accounting for the complex reflectivity of the composite layer. Fourier transform infrared reflectivity (FTIR) measurements, analyzed with the Kramers–Kronig conversion technique, were used to deduce the effective response in reflection of the investigated system. From the knowledge of this phenomenological dielectric function, transversal and longitudinal energy-loss functions were extracted and attributed to transverse and longitudinal resonance modes frequencies.

Keywords: highly doped semiconductors, plasmonic metamaterial, effective dielectric function, effective medium, FTIR spectroscopy

(Some figures may appear in colour only in the online journal)

1. Introduction

Plasmonic metamaterials are opening the door to numerous optical applications due to their unusual physical behaviors and properties that can hardly be found in nature. While a lot of attention is paid to the visible and near-infrared range, pertinent applications reside in the infrared, like gas sensing [1], data storage [2], coherent thermal emission [3] and surface-enhanced infrared absorption (SEIRA) spectroscopy [4–6].

Metals, especially gold and silver, are the primary candidates for plasmonics. However, in the mid-infrared range their supremacy is demoted in favor of highly doped

semiconductors (HDS). In fact, the highly negative permittivity of the metals in this region leads to a reduced skin depth and a large decrease in the electric field exaltation [7, 8]. On the contrary, HDS materials offer the possibility to tune the plasma frequency to a large extent and therefore to adjust the plasmonic resonance frequency in the desired range of application. In this context, recent work has been done on the fabrication of sub-wavelength HDS gratings [9, 10], where the incident light is efficiently coupled to localized surface modes via the large grating momentum. Such devices can exhibit a strong field enhancement in the infrared regime, as required for SEIRA application. In the process of design optimization, an accurate characterization of the resonances

modes is highly desirable. Fourier transform infrared reflectivity (FTIR) has been often used as a non-destructive technique to measure the reflectivity R as a function of the wavelength λ of materials over a wide spectral range. However, determining the resonances associated with high electric field enhancement from such a spectrum is not straightforward. More insight can be obtained using Kramers–Kronig (KK) relations as a conversion technique to deduce the phase shift $\theta(\lambda)$ from the sole amplitude information $\rho(\lambda) = \sqrt{R}$. The KK relations were notably used in this way to study the phonon behavior and charge carrier related properties in semiconductor materials [11–13], powder materials [14] and bulk substrates [15]. Most recently, this approach was used to design an anti-reflection surface [16]. With both reflection amplitude and phase information, the optical properties of thin films can then be obtained [17].

The experimental method we present in this paper first combines FTIR and KK analysis to get the complex reflectivity of a GaSb substrate covered by an HDS subwavelength grating, then the Fresnel equations are used to solve for the complex refractive index of the structured top layer. The phenomenological determination of the effective permittivity of the HDS metamaterial leads to the identification of the plasmonic resonances. The method is first tested numerically by rigorous coupled-wave analysis (RCWA) calculations, showing that effective dielectric functions of the sub-wavelength grating can be extracted for all incidence angles. The approach is then tested experimentally, and resonance modes are identified by determining the phenomenological transverse and longitudinal loss functions. The method then appears as a simple and effective way to determine the resonances of structured surfaces, since there is no exact theory describing the field enhancement and resonances for irregularly shaped particles. As an introduction before the numerical study of the complex HDS structure, the case of a single interface supporting a plasmon polariton is evaluated analytically.

1.1. Effective dielectric function for the surface modes: the case of a single interface

The interest of determining an effective permittivity to identify and describe resonant confined modes can be first exemplified by considering the simplest case of a single interface separating two media (ϵ_1, ϵ_2). The surface mode is characterized by an exponential decay of the field on both sides of the interface. It requires a p-polarized wave to be excited so that the reflectivity can vanish, which can be the case above (Brewster radiation mode) or below the light cone. The well-known dispersion relation matching this condition corresponds to a parallel component of the wave vector $k_{\parallel} = \frac{\omega}{c} \sqrt{\epsilon_s}$, where ω is the frequency of the propagating wave, c is the speed of light and $\epsilon_s = \frac{\epsilon_1 \epsilon_2}{\epsilon_1 + \epsilon_2}$. ϵ_s can be considered, by analogy with the dispersion relation in a bulk material, as the effective dielectric function seen by the radiation or confined Brewster mode. It is instructive to express explicitly the effective permittivity in the case of interest, i.e. for an incident medium corresponding to air

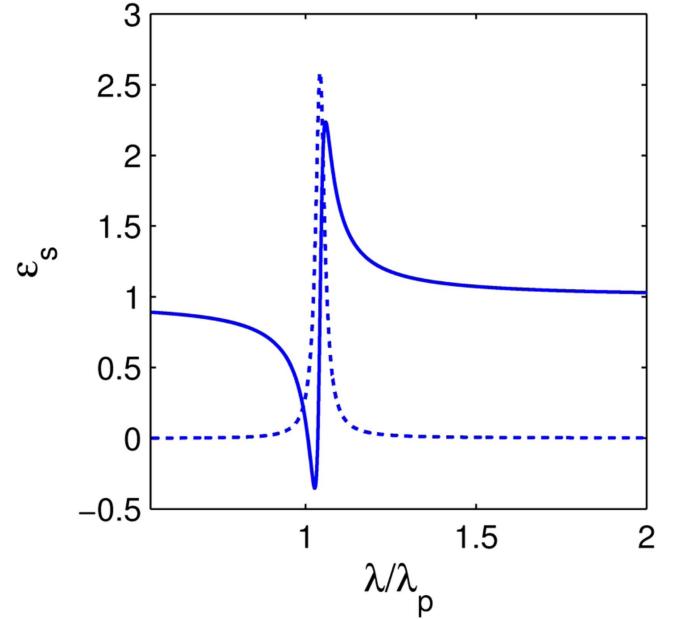


Figure 1. Plot of the effective dielectric function ϵ_s perceived by the radiation Brewster mode and the SPP.

$\epsilon_1 = 1$ and for a sample having a metal-like permittivity. For an HDS, this behavior is observed in the infrared range below the plasma frequency. Figure 1 represents ϵ_s in the case where ϵ_2 is expressed by the Drude model, as follows:

$$\epsilon_2 = \epsilon_{\text{InAsSb}}(\omega) = \epsilon_2^\infty \left(1 - \frac{\omega_p^2}{\omega(\omega + j\gamma_p)} \right) \quad (1)$$

with a plasma frequency corresponding to a wavelength of $5.5 \mu\text{m}$, $\epsilon_2^\infty = 11.7$ and $\gamma_p = 10^{13} \text{s}^{-1}$, corresponding to doping level and damping achievable in highly doped InAsSb [9, 18]. The resulting permittivity ϵ_s corresponds to a single damped Lorentzian oscillator (DLO) revealing the existence of the restoring force at the dielectric/HDS interface. In order to characterize this equivalent oscillator, we need to determine the terms appearing in the dielectric function given by equation:

$$\epsilon_s(\omega) = \frac{\epsilon_1 \epsilon_2(\omega)}{\epsilon_1 + \epsilon_2(\omega)} = \epsilon_{s^\infty} + \frac{S \omega_{TO}^2}{(\omega_{TO}^2 - \omega^2 - i\Gamma\omega)} \quad (2)$$

The ingredients are the high and low frequency limit permittivities ϵ_s^∞ and ϵ_s^{st} , respectively, the oscillator strength $S = \epsilon_s^{st} - \epsilon_s^\infty$, the damping constant Γ , and the transversal resonance frequency ω_{TO} . This is obtained straightforwardly by considering the limit values of ϵ_s , and using the Lyddane–Sachs–Teller relation, $\omega_{TO}^2 = \frac{\epsilon_s^\infty}{\epsilon_s^{st}} \omega_{LO}^2$, we find:

$$\epsilon_s^\infty = \frac{\epsilon_2^\infty \epsilon_1}{\epsilon_2^\infty + \epsilon_1}, \quad \epsilon_s^{st} = \epsilon_1, \quad \Gamma = \gamma_p \quad (3)$$

and

$$\omega_{TO} = \sqrt{\frac{\epsilon_2^\infty}{\epsilon_2^\infty + \epsilon_1}} \omega_p. \quad (4)$$

We recover the Fröhlich frequency $\omega_{TO} = \frac{\omega_p}{\sqrt{2}}$ of a plasma/air interface. This analogy shows that the effective permittivity, ϵ_{eff} gives important quantitative and qualitative information on the considered resonant system, such as the resonance frequency, the sharpness and the intensity of the resonance. For more complex resonators, ϵ_{eff} will not be described by a simple DLO, but the resonant nature of the system is phenomenologically embedded within the notion of effective dielectric function. In the following, we describe the experimental approach we have used to extract the effective optical constants of a metamaterial layer from reflectivity measurement. In this case, ϵ_{eff} is defined as the dielectric function of an homogeneous slab deposited on the same substrate having the same thickness as the meta-layer and providing the same complex reflectivity.

2. Analysis techniques

The analysis techniques that are used and briefed in this section are applied to the infrared reflectivity measurements. As a first step, the phase or the complex argument θ of the reflectivity is calculated from the measured amplitude $\rho = \sqrt{R}$ via the Kramers–Kronig relations. The application of these relations requires some conditions to be satisfied, fortunately the reflectivity function meets these conditions [17]. The KK relations relates the real part $\alpha_1(s)$ to the imaginary part $\alpha_2(s)$ of a function $\alpha(s)$ by:

$$\alpha_2(\omega) = \frac{-2\omega}{\pi} P \int_0^{+\infty} \frac{\alpha_1(s)}{s^2 - \omega^2} ds \quad (5)$$

P denotes the Cauchy principal part of the integral. More detailed theoretical aspects of KK relations are discussed elsewhere [19, 20]. It is important to point out that these KK relations involve an integration from zero to infinity. For this purpose a fit with a sum of Lorentzians (typically five or more) is made at each extremity of the measured spectrum in order to increase the definition range beyond the spectral window. To apply the KK relations, the frequency-dependent reflection coefficient is written as:

$$r(\omega) = \rho(\omega)e^{i\theta(\omega)} \Rightarrow \ln(r(\omega)) = \ln(\rho(\omega)) + i\theta(\omega) \quad (6)$$

Despite its extensive use in the optical constant determination, the drawback of the KK method is that the integration goes in principle from zero frequency to infinity. Since such measurement is not feasible, it is a common practice to fit the spectrum extremities with a Lorentz or Drude-Lorentz model [21], but then the method is necessarily subject to some errors that are not necessarily small. According to KK theorem, the phase equation can be written as:

$$\theta(\omega) = -\frac{1}{2} \int_0^{\infty} \ln \left| \frac{\Omega + \omega}{\Omega - \omega} \right| \frac{d}{d\Omega} [\ln R(\Omega)] d\Omega \quad (7)$$

where Ω is the integration variable. In order to implement KK

integral we write the phase equation in the form:

$$\begin{aligned} \theta(\omega) = & -\frac{1}{2} \left[\int_0^{\Omega_0} \ln \left| \frac{\Omega + \omega}{\Omega - \omega} \right| \frac{d}{d\Omega} [\ln R(\Omega)] d\Omega \right. \\ & + \int_{\Omega_0}^{\Omega_f} \ln \left| \frac{\Omega + \omega}{\Omega - \omega} \right| \frac{d}{d\Omega} [\ln R(\Omega)] d\Omega \\ & \left. + \int_{\Omega_f}^{\infty} \ln \left| \frac{\Omega + \omega}{\Omega - \omega} \right| \frac{d}{d\Omega} [\ln R(\Omega)] d\Omega \right] \quad (8) \end{aligned}$$

where Ω_0 and Ω_f determine the low and high frequency ends of the measured spectrum. We determine $R(\Omega)$ in the first integral of the above equation by extrapolating the measured reflectivity spectrum to zero using the Lorentz–Drude model. Then, the first integral in the phase equation can be readily solved. To solve the second integral, we write it in the form:

$$\int_{\Omega_0}^{\Omega_1} + \int_{\Omega_1}^{\Omega_2} + \dots + \int_{\Omega_i}^{\Omega_{i+1}} + \dots + \int_{\Omega_{f-1}}^{\Omega_f} \quad (9)$$

in each interval $[\Omega_{i-1}, \Omega_i]$ (which determines the experimental spectral resolution), we approximate the reflectivity with a linear fit. Then, we obtain the value of the second integral by solving each elementary integral numerically and summing over all the individual integrals. We determine the analytical expression of $R(\omega)$ in the third integral by extrapolating the reflectivity spectrum to infinity using pure mathematical functions, and then we solve the third integral numerically. We believe that the arbitrary extrapolation of the reflectivity in the third integral is the only source of error in the determination of the phase. Therefore, we believe that the error on the overall phase is not angle-dependent. It depends on the variation of the reflectivity spectrum beyond the measured frequency range. If the reflectivity spectrum saturates beyond the measured frequency range, the contribution of the third integral to the overall phase is nil, and the phase obtained by the KK conversion technique is highly accurate. However, if the reflectivity spectrum beyond the measured frequency range varies, the contribution of the third integral to the overall phase in the measured frequency range is a slightly increasing angle as we move towards the high frequency end of the measured spectrum.

As a second step, the transfer matrix model (TMM) is used to determine the effective optical constants of the structured HDS layer, without any physical assumption. We consider that the top layer, consisting of HD InAsSb grating and air, has an effective index of refraction N_l . The complex index of refraction of the GaSb substrate N_s is taken from literature [22]. The expression of light reflection on the system can be found in many textbooks [23, 24], and is written as:

$$\ln(r(\omega)) = A(N_l, N_s) + iB(N_l, N_s) \quad (10)$$

We then equate the real and imaginary parts of equations (6) and (10), with the only unknown parameter $N_l = n_l + ik_l$. The dependence of these two equations on the unknown parameter N_l is non-trivial. Thus, we vary n_l and k_l until we solve the two equations simultaneously. The accuracy is specified by the variation step.

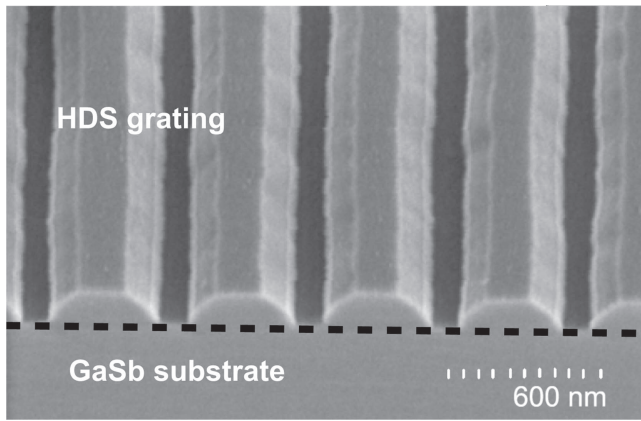


Figure 2. SEM image of the studied InAsSb grating.

3. Experiments

The FTIR system used is a Nicolet 4700 spectrometer from Thermo Electron Corporation with a DTGS detector and a KBr beam-splitter, working between 400 and 4000 cm^{-1} at near normal incidence. We performed 200 scans on the sample in order to improve the signal-to-noise ratio while fixing the spectral resolution to 1 cm^{-1} . Because the sample compartment is not evacuated, there needs to be a relative scale for the absorption intensity. Thus, we use a gold coated mirror to collect a background spectrum before each measurement. The spectrum of the sample is then normalized to this background to remove the instrumental and environmental contributions. Thus, all spectral features present in the normalized spectrum are strictly due to the sample. Parameters adjustment and data acquisition are made by OMNIC software.

The InAsSb layer is n-doped with Si at a doping concentration of $5 \times 10^{19} \text{ cm}^{-3}$. It is deposited by molecular-beam epitaxy on GaSb doped with Te at a doping concentration of $2 \times 10^{18} \text{ cm}^{-3}$. A SiO_2 mask is deposited on the top. The grating is then defined by holography using an AZMIR 701 positive photoresist, followed by reactive chemical etching. The final shape of the lines is trapezoidal with base length of 420 nm, top length 120 nm and height of 140 nm. The period of this grating is 520 nm. Figure 2 shows an SEM image of the obtained structures. Such structures exhibit strong field enhancement and were made based on prospective application in SEIRA. InAsSb material was used because of the impressive doping level it offers, giving the possibility to tune the bulk plasma wavelength down to values as low as 5 μm . The effective mass of electrons in InAs is also small in comparison to other HDS; such small effective mass promotes the ability to increase the plasma frequency. In addition, the InAsSb is lattice-matched with the GaSb substrate, ensuring high quality epitaxy.

4. Results and discussion

4.1. Numerical calculation: angle dependence study

In this section, we aim to study our resonant system at different excitation angles to verify the best configuration to

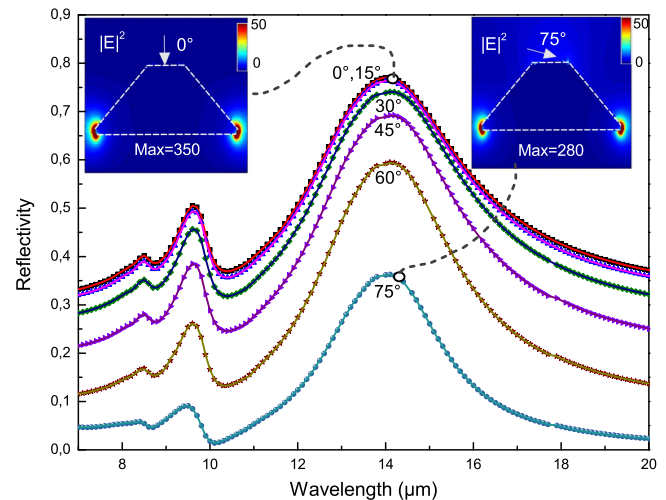


Figure 3. Initial reflectivity in symbols, and the corresponding back-calculated one in solid line as a function of wavelength and angle of incidence. The insets show normalized intensity maps at the frequencies where the enhancement factor is maximum (350 and 280 at normal and grazing angles, respectively). The images are saturated for a better visualization of the light distribution.

excite the surface localized plasmon resonances (LSPR) and to assess the validity of applying our method to plasmonics and show its accuracy. For this purpose, numerical simulations on a configuration that resembles the actual structures, i.e. a trapezoidal shape with a base length of 420 nm, top length of 120 nm and height of 140 nm, were made (inset figure 3). The incident angle varies from 0 to 75 deg. The index of refraction of the substrate GaSb was implemented as found in the literature [22]. The index of refraction of the HDS was modeled using the Drude model as in equation (1), with the same parameters. The Drude model describes well the optical properties of a material when these properties are essentially driven by the conduction band electrons. In the InAsSb:Si sample the electron density is close to 10^{20} cm^{-3} . Even if the band gap is around 0.3 eV [25] because of the Burstein–Moss shift [26] the effective band gap becomes close to 1 eV removing interband and intraband transition; thus, in the mid-infrared, the Drude model accounts precisely for the optical response of HDS [10, 27]. Though it is important to point out that the Drude model is only used in simulations to better understand the LSPR behavior. The developed method extracts the complex permittivity without any physical assumption. The RCWA method was used to calculate directly the complex reflectivity at each angle of incidence, the reflectivity is shown in figure 3. While the spectrum exhibits clear maxima, it is difficult to infer unambiguously the maximum resonance wavelength of the system. For example, plasmonic resonances can be associated with reflectivity minima, as is the case in the Kretschmann configuration. In fact, the resonance wavelengths of LSPR are well correlated with the positions of the absorption maxima in such dissipative systems. Although scattering or absorption spectra $A(\lambda)$ are often difficult to obtain experimentally, this information can also be calculated numerically. In the present

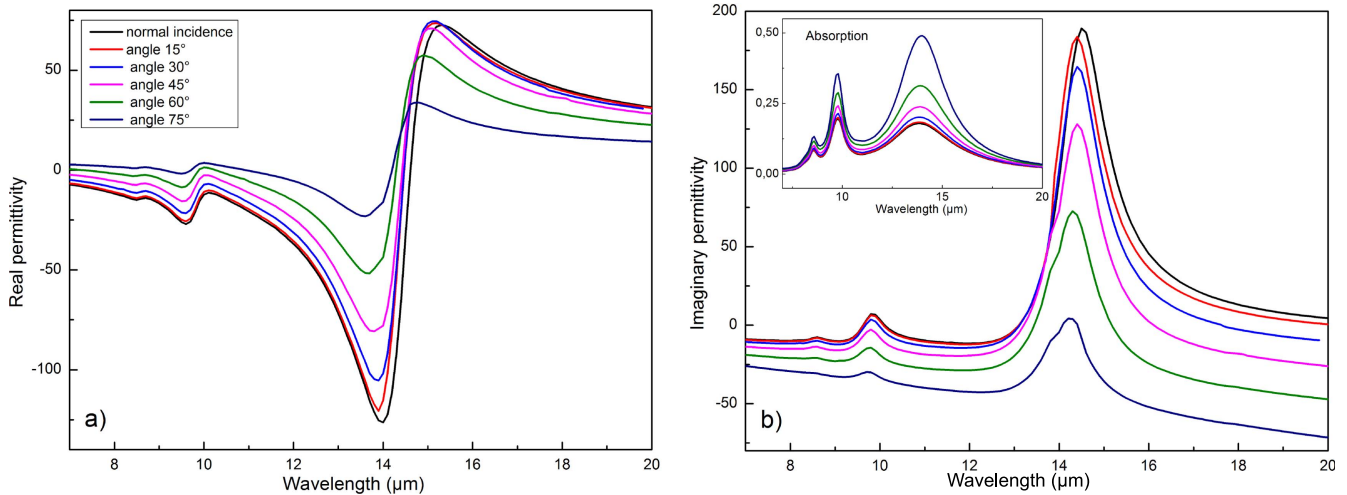


Figure 4. (a) Real and (b) imaginary parts of the permittivity of the effective layer as a function of wavelength and angle of incidence. The inset shows the absorption as a function of angle calculated by RCWA.

configuration, the light impinging from the air is mostly specularly reflected, transmitted or absorbed given the sub-wavelength size of the structures in the mid-IR. Hence, $A(\lambda)$ is quite precisely given by $1 - R(\lambda) - T(\lambda)$, where $T(\lambda)$ is the transmission of the structured layer on the GaSb substrate. The absorption is shown in the inset of figure 4(b) revealing the presence of more pronounced peaks, only slightly shifted compared to the reflection maxima. While a square cross-section of similar size produces only one strong resonance above the plasma frequency at normal incidence (not shown here), the reduced symmetry of the trapezoidal shape produces additional, less intense peaks, that are blue-shifted compared to the main peak. The intensity maps clearly show that these modes correspond to an excitation mostly localized at the structure basis (see insets of figure 3) which is maximum at normal incidence in terms of field enhancement. The TMM was then applied following the mentioned procedure to combine the contribution of substrate with that of the film, allowing us to determine the effective refractive index of the top layer from the calculated reflectivity. The corresponding dielectric function is deduced from $\epsilon = \frac{1}{\mu}(n + ik)^2 \approx (n + ik)^2$, i.e. we considered $\mu \approx 1$. This is not a rigorous approach, since even if we started with a non-magnetic material, the structuring may introduce some magnetic behavior; however, the variation of μ is expected to be reasonably small for the investigated structures, that were not designed to produce a magnetic resonance related to a current loop (as in some thick metallic nano-rings [28]).

Figure 4 shows the real and imaginary parts of the retrieved dielectric function for increasing angles of incidence. Lorentzian-like resonances are clearly visible. The resonant behavior is seen for all angles of incidence as expected since LSPR typically does not require stringent illumination conditions to be excited. However, the dielectric function resonance is more pronounced for normal incident angle, where the horizontal polarization efficiently excites the plasmonic mode confined on the lateral edges of the structures. Comparing the absorption calculated by RCWA for the system, inset in 4(b), to the imaginary part of the permittivity

calculated by TMM figure 4(b), we notice the presence of similar peaks with interesting differences. We note that, when the absorption is strong (at large angle), the imaginary part of the dielectric function has a minimal amplitude and vice versa. This can be understood if we consider that the large absorption obtained at large angle corresponds to a more damped oscillator. In fact, if the light is indeed more absorbed at large angle (whatever the wavelength) since the light perceives more HDS material, the maximum resonance actually occurs at normal incidence as previously mentioned. In this sense, the effective permittivity appears as a better indicator of resonance strength.

Figure 3 shows the back-calculated reflectivities as function of angle, in solid lines, using the values obtained in figure 4 compared to the initial reflectivities, shown as symbols. We notice the good agreement and the high precision of our calculation. However, it should be noted that in this phenomenological approach, the effective layer thickness is arbitrarily taken as equal to the grating thickness. Other thicknesses can lead to noticeable changes in the retrieved complex index without considerably affecting the obtained Lorentz-like behavior and the general trend. We can note also that for steep angles and high wavelength the solutions for the imaginary part of the refractive index are negative. This is, however, acceptable since it only means that in this region the metamaterial reflects the wave as a certain homogeneous gain layer would do. In other words, the obtained effective constants account for the reflection response and should not be used, for example, to quantitatively infer the transmission response.

4.2. Application to FTIR measurement

FTIR measurement was done on the sample shown in figure 2 at quasi-normal incident IR-beam with p-polarization. KK relations were applied to obtain the complex part θ in equation (6); extrapolation has been performed at the extremities. TMM has been then applied to obtain the complex index of refraction of the top layer made of InAsSb air,

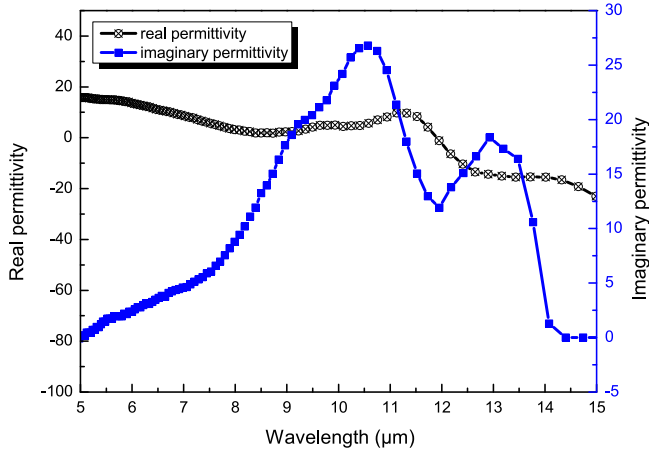


Figure 5. Real part of the dielectric function of the effective layer (black) along with its imaginary part (blue).

sandwiched between the GaSb substrate and air. Figure 5 shows the complex permittivity calculated using the obtained real refractive index, n , and the extinction coefficient, k . We see that the real part of the permittivity goes from positive to negative, exhibiting a damped resonant behavior.

To check the validity of these solutions, the effective permittivity shown in figure 5 was used to back calculate the reflectivity. Figure 6 shows the measured reflectivity along with the back-calculated reflectivity. A very satisfactory agreement is observed as all the experimental reflectivity features were retrieved.

We must point out that a constant term of 0.4 rad was added to the values of θ so that the obtained back reflectivity is optimum. This term is regarded as a constant correction to KK relations. Two factors involved in our experiment might be the reason behind the necessity of this correction term. The first reason comes from the fact that the permittivity function for the substrate was used from the literature, while the actual substrate is Te doped with plasma wavelength of 30 μm . This introduces a sharp non-accounted-for decrease at wavelengths of 20 μm , more details are found in [9]. The second reason might stem from overestimation or underestimation of the reflectivity while extrapolating at zero frequency and at infinity.

In order to show the TO- and LO-like resonances typically associated with Lorentzian permittivities, it is useful to introduce the two ‘loss functions,’ often used in thin films analysis and expressed in detail elsewhere [29]. The first one is called the ‘TO energy loss function’:

$$\text{TO energy loss function}(\omega) = \text{Im}(\epsilon(\omega)) \quad (11)$$

The maxima of this function corresponds to the resonance frequencies of TO vibrations. The ‘LO energy loss function’ is defined as:

$$\begin{aligned} \text{LO energy loss function}(\omega) &= \text{Im}\left(-\frac{1}{\epsilon(\omega)}\right) \\ &= \frac{\epsilon''(\omega)}{\epsilon'^2(\omega) + \epsilon''^2(\omega)} \end{aligned} \quad (12)$$

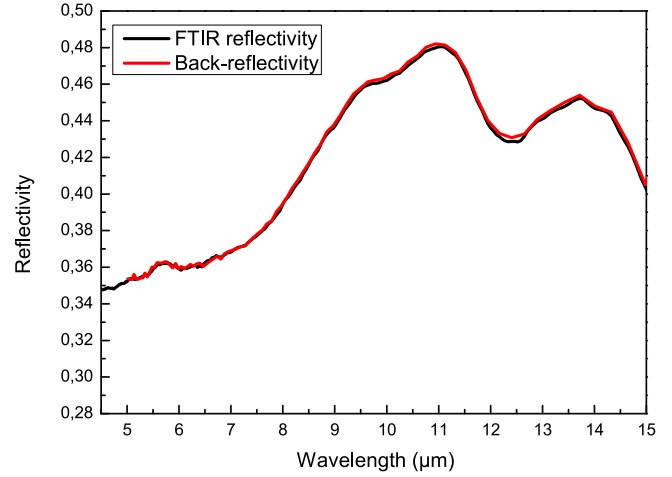


Figure 6. FTIR reflectivity spectrum along with the back-calculated reflectivity, calculated using values in figure 5.

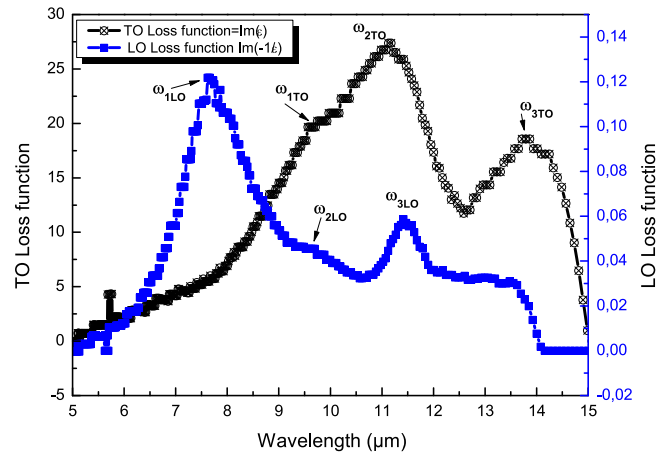


Figure 7. TO loss function showing TO resonance frequencies as well as LO loss function showing the LO resonance frequencies.

where $\epsilon'(\omega)$ and $\epsilon''(\omega)$ are the real and imaginary parts of the permittivity, respectively. By definition, the maxima of this function occur at the resonance frequencies of the LO vibrations of the medium.

From figure 7 we have a clear idea about the peak positions of LO and TO vibrations. As we can see, we have three resonance frequencies corresponding to the TO vibrations, $\omega_{1TO} \approx 9.7 \mu\text{m}$, $\omega_{2TO} \approx 11.1 \mu\text{m}$, and $\omega_{3TO} \approx 13.8 \mu\text{m}$. We notice two strong LO vibrations peaks $\omega_{1LO} \approx 7.9 \mu\text{m}$ and $\omega_{2LO} \approx 10.1 \mu\text{m}$ and one strongly-damped LO vibrations peak at $\omega_{3LO} \approx 12 \mu\text{m}$. We notice that there is a marked splitting in the resonance frequency of the sample, as expected for non-rectangular shapes of ribbons [9]. As obtained in the simulations, the symmetry reduction produces this degeneracy lifting of the TO resonance.

5. Conclusion

A general approach was tested in order to retrieve effective optical constants of an MM layer deposited on a known substrate, from the knowledge of the complex reflectivity

spectrum at a given angle. The technique was validated numerically and experimentally on an HDS subwavelength grating. The simulations showed that for each angle the reflection response is faithfully accounted for by a homogeneous layer having an angle-dependent effective dielectric function. This quantity provides unambiguously the signatures of the LSPR through resonances having DLO-like shape. Using KK relations we were able to determine experimentally the resonance frequencies in an HDS grating; accurate results were manifested through the back calculation of the experimental reflectivity. The nature of the resonance frequencies were pointed out using the LO and TO loss functions. We observed that the resonance intensities are clearly indicated by the strength of the oscillator, information which is not directly obtained from the sole reflection or absorption spectrum.

Acknowledgments

This work was supported by the nano'mat platform, the French Investment for the Future Program (EquipEx EXTRA, ANR 11-EQPX-0016), the French ANR (SUPREME-B, ANR-14-CE26-0015), the European Unions Horizon 2020 research and innovation programme (Marie Skłodowska-Curie grant agreement No 641899) and by the ARPE programme from 'la region Occitanie'. Vilianne Ntsame Guilengui is acknowledged for the fabrication of the semiconductor grating, used for the experimental sensing demonstration in this article.

References

- [1] Rodrigo D, Limaj O, Janner D, Etezadi D, de Abajo F J G, Pruneri V and Altug H 2015 Mid-infrared plasmonic biosensing with graphene *Science* **349** 165–8
- [2] Ocelic N and Hillenbrand R 2004 Subwavelength-scale tailoring of surface phonon polaritons by focused ion-beam implantation *Nat. Mater.* **3** 606–9
- [3] Greffet J-J, Carminati R, Joulain K, Mulet J-P, Mainguy S and Chen Y 2002 Coherent emission of light by thermal sources *Nature* **416** 61–4
- [4] Anderson M S 2005 Surface enhanced infrared absorption by coupling phonon and plasma resonance *Appl. Phys. Lett.* **87** 144102
- [5] Anderson M S 2003 Enhanced infrared absorption with dielectric nanoparticles *Appl. Phys. Lett.* **83** 2964–6
- [6] Bjerke A E and Griffiths P R 2002 Surface-enhanced infrared absorption spectroscopy of p-nitrothiophenol on vapor-deposited platinum films *Appl. Spectrosc.* **56** 1275–80
- [7] Soref R, Hendrickson J and Cleary J W 2012 Mid-to long-wavelength infrared plasmonic-photonics using heavily doped n-Ge/Ge and n-GeSn/GeSn heterostructures *Opt. Express* **20** 3814–24
- [8] Li D and Ning C Z 2011 All-semiconductor active plasmonic system in mid-infrared wavelengths *Opt. Express* **19** 14594–603
- [9] N'Tsame Guilengui V, Cerutti L, Rodriguez J-B, Tournié E and Taliercio T 2012 Localized surface plasmon resonances in highly doped semiconductors nanostructures *Appl. Phys. Lett.* **101** 161113
- [10] Taliercio T, Guilengui V N, Cerutti L, Tournié E and Greffet J-J 2014 Brewster mode in highly doped semiconductor layers: an all-optical technique to monitor doping concentration *Optics Express* **22** 24294–303
- [11] Collins A T, Lightowers E C and Dean P J 1967 Lattice vibration spectra of aluminum nitride *Phys. Rev.* **158** 833–8
- [12] Zhiqiang Y and Harding G L 1984 Optical properties of DC reactively sputtered thin films *Thin Solid Films* **120** 81–108
- [13] Kazan M, Ottaviani L, Moussaed E, Nader R and Masri P 2008 Effect of introducing gettering sites and subsequent Au diffusion on the thermal conductivity and the free carrier concentration in n-type 4H-SiC *J. Appl. Phys.* **103** 053707
- [14] Pecharromán C, Gonzalez-Carreno T and Iglesias J E 1995 The infrared dielectric properties of maghemite, γ -Fe₂O₃, from reflectance measurement on pressed powders *Phys. Chem. Miner.* **22** 21–9
- [15] Barker A S Jr and Hopfield J J 1964 Coupled-optical-phonon-mode theory of the infrared dispersion in BaTiO₃, SrTiO₃, and KTaO₃ *Phys. Rev.* **135** A1732
- [16] Horsley S A R, Artoni M and Rocca G C L 2015 Spatial Kramers–Kronig relations and the reflection of waves *Nat. Photon.* **9** 436–9
- [17] Rahbany N, Kazan M, Tabbal M, Tauk R, Jabbour J, Brault J, Damilano B and Massies J 2013 Measurement of the effect of plasmon gas oscillation on the dielectric properties of p- and n-doped Al_xGa_{1-x}N films using infrared spectroscopy *J. Appl. Phys.* **114** 053505
- [18] Guilengui V N 2013 Technologie et étude de résonateurs plasmoniques à base d'InAsSb: vers une plasmonique tout semi-conducteur *PhD thesis* Université Montpellier 2
- [19] Jasperse J R, Kahan A, Plendl J N and Mitra S S 1966 Temperature dependence of infrared dispersion in ionic crystals LiF and MgO *Phys. Rev.* **146** 526
- [20] Popović Z V, Stanišić G, Stojanović D and Kostić R 1991 Infrared and raman spectra of CdO *Phys. Status Solidi b* **165** K109–12
- [21] Kuzmenko A B 2005 Kramers-kronig constrained variational analysis of optical spectra *Rev. Sci. Instrum.* **76** 083108
- [22] Adachi S 1987 Model dielectric constants of GaP, GaAs, GaSb, InP, InAs, and InSb *Phys. Rev. B* **35** 7454
- [23] Heavens O S 1960 Optical properties of thin films *Rep. Prog. Phys.* **23** 1
- [24] Yeh P 1988 *Optical Waves in Layered Media* vol 95 (New York: Wiley)
- [25] Webster P T, Riordan N A, Liu S, Steenbergen E H, Synowicki R A, Zhang Y-H and Johnson S R 2015 Measurement of inasb bandgap energy and inas/inasb band edge positions using spectroscopic ellipsometry and photoluminescence spectroscopy *J. Appl. Phys.* **118** 245706
- [26] Burstein E 1954 Anomalous optical absorption limit in insb *Phys. Rev.* **93** 632
- [27] Taliercio T, N'Tsame Guilengui V, Cerutti L, Rodriguez J-B, Barho F, Rodrigo M-J M, Gonzalez-Posada F, Tournié E, Niehle M and Trampert A 2015 Fano-like resonances sustained by si doped inasb plasmonic resonators integrated in gasb matrix *Opt. Express* **23** 29423–33
- [28] Smith D R, Schultz S, Markoš P and Soukoulis C M 2002 Determination of effective permittivity and permeability of metamaterials from reflection and transmission coefficients *Phys. Rev. B* **65** 195104
- [29] Tolstoy V P, Chernyshova I V and Skryshevsky V A 2003 *Handbook of Infrared Spectroscopy of Ultrathin Films* (New York: Wiley) (<https://doi.org/10.1002/047123432X>)